

Crack Detection in High Strain Aerospace Applications¹

S.R. Soni², E.D. Swenson³ and R.T. Underwood⁴

Abstract: Detecting through-thickness fatigue cracks in a geometrically constrained structure is a challenging structural health monitoring (SHM) problem due to potentially degraded sensor performance. Fatigue cracks are typically found in aircraft structures during visual inspections and non-destructive testing (NDT); however, there exists a real need to detect damage between NDT intervals. Over the last decade, a significant amount of research effort has been focused on developing “hot spot” approaches to monitor areas of structures known to have damage using Lamb waves generated from surface-mounted lead zirconate titanate (PZT) transducers. This research is focused on evaluating an SHM approach for detecting fatigue cracks in a “hot spot” that takes into account tight geometric constraints and changes in sensor performance due to high strain levels and high-cycle fatigue, so as to maintain a high probability of damage detection. In order to account for changes in PZT performance due to high-cycle fatigue and static loads, relative changes in signals from a reference pair of PZTs mounted in close proximity are removed from measured test signals. These relative changes indicate that fatigue cracks can in many cases be sensed under various loads even after considerable sensor degradation.

Keywords: Structural Health Monitoring, Lamb waves, fatigue crack, PZT sensors

1 Introduction

The “health” of an aircraft’s structure determines its overall readiness and its ability to perform a required mission. Typically, backshop maintenance performs struc-

¹ The views expressed in this article are those of the authors and do not reflect the official policy or position of the Air Force, Department of Defense or the U.S. Government

² Department of Systems Engineering and Management, U.S. Air Force Institute of Technology, Wright-Patterson AFB, OH, USA.

³ Department of Aeronautics and Astronautics, U.S. Air Force Institute of Technology, Wright-Patterson AFB, OH, USA.

⁴ U.S. Air Force Non-Destructive Inspection Program Office, Tinker AFB, OK, USA.

tural health assessments on each aircraft so as to provide data regarding the structural health of the fleet. With the application of structural health monitoring (SHM) systems, it may be possible for maintainers to uninterruptedly monitor an aircraft's structural health without impacting aircraft readiness. If maintenance is only performed when required - known as the condition based maintenance paradigm - as opposed to servicing at a fixed interval, aircraft readiness could increase and sustainment costs would likely decrease.

Over the last decade, a significant amount of research effort has been focused on developing SHM approaches for "hot spots", or areas of structures where damage is known to have occurred, using Lamb waves generated from surface-mounted lead zirconate titanate (PZT) transducers. Bonding PZT transducers to the surface of a plate and creating Lamb waves by applying an electric charge across the PZT wafer is a common approach in SHM systems. A "pitch-catch" approach is utilized in this research, where Lamb waves are created (pitched) by one PZT and measured (caught) by another, to detect cracks in an aluminum plate that is sized to represent an aircraft bulkhead section. In the next section, a background discussion on SHM approaches applied to aerospace vehicles is provided followed by a detailed description of the experiment.

2 Background

The following discussion is focused on previous SHM approaches that use Lamb waves to detect damage in aerospace applications. Malkin, Leonard, Derriso, and Haugse [Malkin, Leonard, Derriso, and Haugse (2007)] recently introduced a framework for the development of "hot spot" monitoring specifically for aircraft. Kessler, Amaratunga, and Wardle [Kessler, Amaratunga, and Wardle (2005)] studied sensor durability and discussed various durability standards for commercial and military aircraft components and how they relate to aircraft SHM systems. Kessler and Shim [Kessler and Shim (2005)] created an SHM system specifically designed for aircraft systems called the Monitoring & Evaluation Technology Integration Disk (M.E.T.I.-Disk) and demonstrated its capability to detect the presence and location of damage. Lu, Ye, Su, and Yang [Lu, Ye, Su, and Yang (2008)] studied the interaction of Lamb wave modes at a variety of excitation frequencies with a through-thickness crack in aluminum plates at various angles. They found that wave scattering from a crack leads to complicated transmission, reflection, and diffraction accompanied with mode conversion. To assist in clear identification of crack-scattered waves, they applied a dual PZT actuation scheme to generate S_0 modes only. Swenson and Crider [Swenson and Crider (2007)] evaluated a pitch-catch approach to detect damage in a simulated aircraft bulkhead with electrical discharge machine (EDM) notches added to simulate damage. As an extension to

Swenson and Crider's previous research, Underwood, Swenson, and Soni applied similar SHM techniques on real cracks propagated in a test article [Underwood, Swenson, and Soni (2008)]; however, this work could not conclusively show that damage was detected until the effects of PZT degradation could be removed from sensor measurements. The focus of the present research is to extend this work by removing the effects of sensor degradation due to static and cyclic loads, which is discussed next.

PZT degradation due to high strain and cyclic loading has been studied by several authors. Kuhn [Kuhn (2009)] studied performance, durability, and reliability of SHM systems in a hostile aircraft environment. In his research, he conducted 870 hours of testing, 110 hours of data collection, and tested 120 conditions related to PZT sensor degradation due to high-cycle fatigue. Using the statistical software package JMP®, he fit a power model equation to his measured data over a range of 800 to 2,600 microstrain ($\mu\epsilon$) and 0 to 510,000 load cycles, which he defined the integrated sensor magnitude $R(c, s)$ as

$$R(c, s) = 112.63 * \left[\frac{c}{1000} \right]^{-2.125 * 10^{-5} s + 0.009752} \quad (1)$$

where c is the number of load cycles and s is the strain level in $\mu\epsilon$. Sensor signal degradation predicted by Eq. (1) is directly compared to the measured signal degradation seen in this research because Kuhn conducted his research using the same APC 850 PZTs, grade of aluminum, and PZT adhesive. However, there are limits to the applicability of Kuhn's sensor degradation equation because Eq. (1) was fit to data collected at cyclic strain levels between 800 and 2,600 $\mu\epsilon$. The research presented in this paper exceeds the strain region that Kuhn studied.

Kusaka and Qing [Kusaka and Qing (2003)] studied PZT performance under monotonic and fatigue loading on composite and aluminum structures. They compared healthy and damaged peak-to-peak signal magnitudes over a static strain range of 0 to 17,500 $\mu\epsilon$ and fatigue loading tests in a strain range of 0 to 15,000 $\mu\epsilon$ and up to 10^6 fatigue load cycles. They found that PZT performance remained unchanged if the applied static strain did not exceed the manufacturer's defined static failure strain limit; however, if the applied strain exceeded this limit, Kusaka and Qing found that PZT performance degraded as a function of both strain and fatigue cycles. Blackshire, Martin, and Na [Blackshire, Martin, and Na (2007)] studied the degradation of surface-bonded PZTs and various PZT bonding materials under static and low frequency loadings. They noted a link between the bond material and PZT damage, and found that when the bond is non-compliant sensor cracking, fracture, and disbond directly affected the sensor's performance.

In the next section, we will discuss the experimental setup and test article on which

an SHM approach for detecting fatigue cracks in a “hot spot” is evaluated. This approach takes into account tight geometric constraints and changes in sensor performance due to high strain levels and high-cycle fatigue. Ultimately, this research shows that cracks can in many cases be sensed under various loads even after considerable sensor degradation.

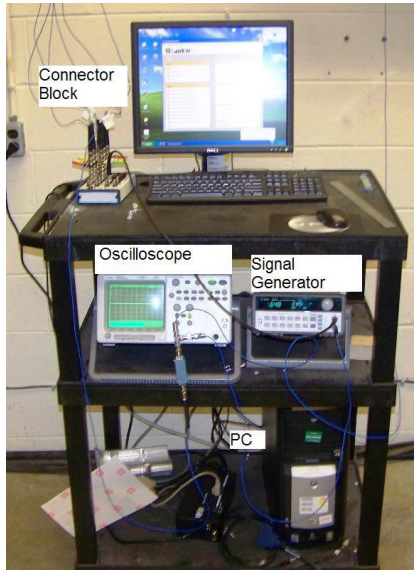


Figure 1: Data collection system

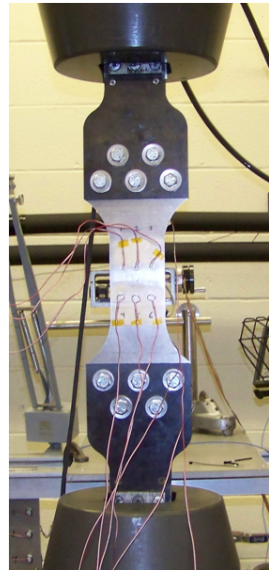


Figure 2: Dog bone test article in MTS

3 Experiment and Analysis Approach

3.1 Test Setup

The primary test equipment used in this experiment is shown in Fig. 1 which includes an Agilent 33120A arbitrary waveform generator, a Hewlett Packard 54621A oscilloscope, and a National Instruments PCI-6133 data acquisition (DAQ) card set to sample at 2.5 MHz while recording up to eight signals simultaneously. The experiment operates in a LabVIEW® environment in which the waveform generator creates a 5.5 cycle Hanning-windowed sine wave over a frequency range of 50 kHz to 500 kHz in 10 kHz increments. The model 850 American Piezo Ceramics 6.35 mm diameter PZT discs act as both actuators and sensors. The PZTs are bonded to the surface of the test article using M-Bond 200 adhesive and connected with shielded coaxial cables to the waveform generator and DAQ card.

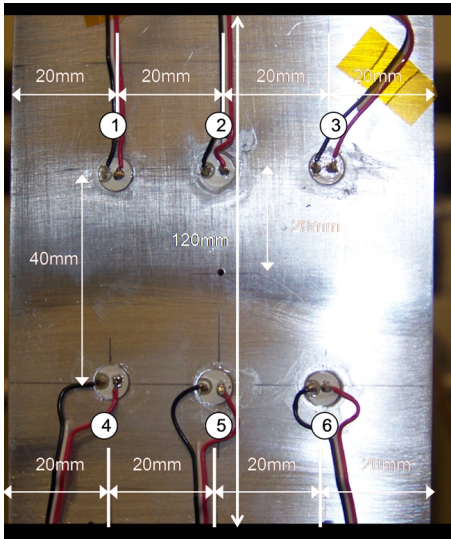


Figure 3: Photograph of the front of the test article (undamaged - only hole present)

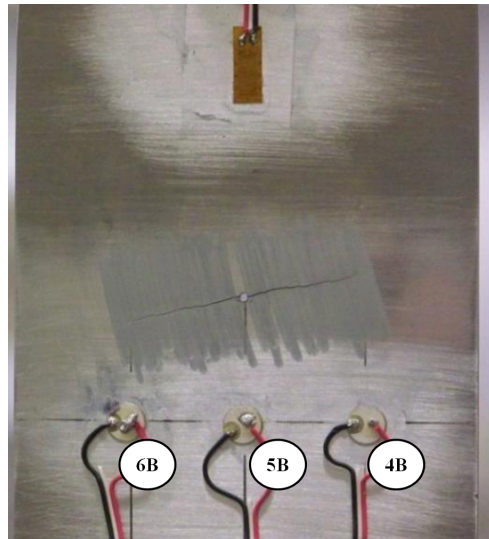


Figure 4: Photograph of the back of test article showing PZTs, strain gauge, and crack extending from hole

3.2 Test Article

The test article is an 3.175 mm thick 6061-T6 aluminum dog bone test coupon with an overall test area of 80 mm x 120 mm (see Figs. 2, 3, and 4). The rows of PZTs are 40 mm apart, which represents the expected placement of PZTs in a real application. A total of nine PZTs are attached to the test article, six on the front side (PZTs 1 through 6) and three on the back (PZTs 4B, 5B, and 6B). Additionally, there is a standard 1-axis strain gage, rated to 5,000 $\mu\epsilon$, located on the back of the plate (see top of Fig. 4).

To detect damage, a pitch-catch approach is used where PZTs 1, 2, and 3 (as shown in Figs. 2) and 3, are the actuators that create the Lamb waves and PZTs 4, 5, 6, and PZTs 4B, 5B, and 6B (as shown in Figs. 4 and 3 respectively) are used to sense the Lamb waves. Since all responses are collected in pitch-catch pairs, the excitation PZT is always listed first and the sensing PZT is listed second. For example, a signal collected from PZT pair 1-5 means the excitation PZT is 1 and sensing PZT is 5. PZTs 4B, 5B, and 6B are located directly opposite PZTs 4, 5, and 6 on the back of the test plate in order to determine Lamb wave mode by determining the symmetry or asymmetry between the signals collected from PZTs opposite each other.

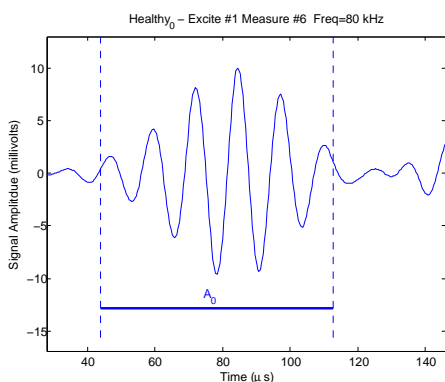


Figure 5: Measured waveform from an 80 kHz excitation and theoretical A_0 mode arrival window

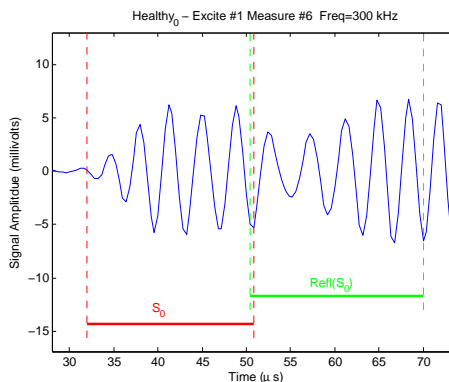


Figure 6: Measured waveform from an 300 kHz excitation and theoretical S_0 and S_0 windows

The test article has a 1.67 mm diameter simulated rivet hole in its center from which fatigue cracks propagate (see Fig. 3). Cyclic loading is applied by a 810 Material Test System (MTS) 110 kip hydraulic test machine at a rate of 4 Hz for all load cycles. To detect the damage, PZTs 1, 2, and 3 are excited in turn while measuring responses at PZTs 4, 4B, 5, 5B, 6, and 6B simultaneously. To increase the probability of detecting the presence of a crack, the crack size is opened by increasing the static load [Olson, DeSimio, and Derriso (2006); Adams (2007)]. Therefore, the data is collected under four static loads: 0.45, 17.8, 26.7, and 35.6 kN. A 10X telescopic lens is used to measure the horizontal length of the crack to an accuracy of 0.01 mm. The crack length is measured from tip to tip and includes the diameter of the simulated rivet hole.

3.3 Response Windows

In structures with restricted geometry, discerning different Lamb wave modes can be difficult because reflected Lamb packets result in PZT signals that can be challenging to interpret. Both the fundamental symmetric S_0 and antisymmetric A_0 Lamb wave modes are generated and higher modes are avoided by keeping the frequency-thickness product below 1.5 MHz-mm; therefore, the excitation frequency is kept below 500 kHz for the 3 mm thick test article. Time-of-flight (TOF) windows of Lamb wave packets, as shown in Figs. 5 and 6, are computed by first spectrally decomposing an input signal into its constitutive harmonic components and then propagating these components over the distance using each component's appropriate phase velocity. A time domain signal is then reconstructed, and the

TOF window or window length of the wave packet is computed. This approach for predicting the window length accurately takes into account the dispersive effects - wave speed being a function of frequency - of Lamb waves.

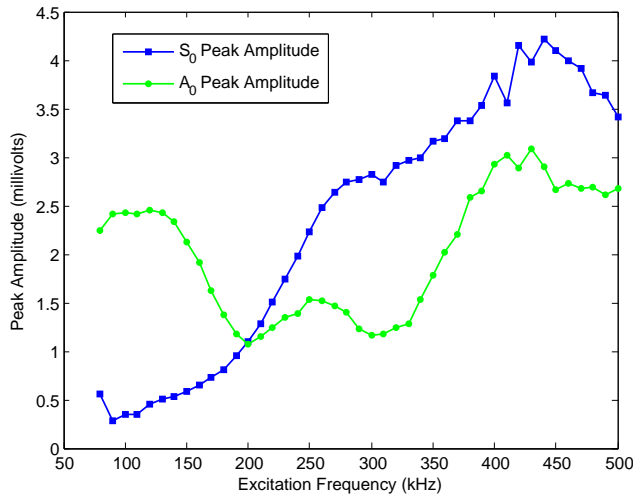


Figure 7: Measured S_0 and A_0 maximum PZT amplitude versus frequency for a 3 mm plate

The difference in the arrival time between the direct S_0 and first reflected S_0 packet varies with excitation frequency, distance between PZTs, and distance to an edge from which the S_0 packets reflect. In order to exclude the first reflected S_0 mode, the S_0 mode TOF window is reduced. This window reduction varies approximately linearly starting from a maximum of 44% reduction in window length at 190 kHz to almost no reduction at 300 kHz, as shown in Fig. 6. No reduction in window length is required for excitation frequencies higher than 300 kHz. This window reduction is particularly important because reflected waves could propagate along a path that avoids damage, and therefore lead to false negative indications of damage [Swenson and Crider (2007)]. The A_0 TOF window is not reduced because the S_0 mode amplitude is generally lower than the A_0 mode between 80 and 200 kHz as shown in Fig. 7. Underwood [Underwood (2008)] created Fig. 7 from results collected in an experiment where he isolated and measured the peak signal magnitude of each Lamb wave mode as a function of frequency in a 610 mm by 1,210 mm by 3 mm thick aluminum plate. The dog bone test specimen for this experiment was later cut from Underwood's test plate.

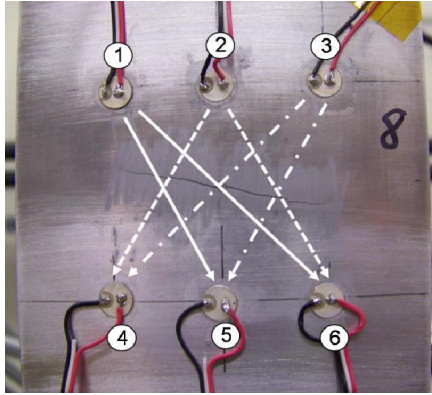


Figure 8: Propagation paths between PZTs that cross damaged areas

3.4 Damage Detection

The approach taken to detect damage is to compare relative changes in the integrated responses of the test and reference PZT pairs in the predicted TOF windows. The integrated or summed response A_{p-c} of PZT pair $p-c$ for the A_0 mode is defined for excitation frequencies 80 to 200 kHz as

$$A_{p-c} = \left[\sum_{i=t_a}^{t_b} x_i^2 \Delta t \right]^{1/2} \quad (2)$$

where t_a is the arrival time of the direct A_0 packet, t_b is the end time of the A_0 packet, and Δt is 400 ns because all data was collected at 2.5 MHz. The integrated or summed response S_{p-c} for the S_0 mode is defined for excitation frequencies from 210 to 500 kHz as

$$S_{p-c} = \left[\sum_{i=t_c}^{t_d} x_i^2 \Delta t \right]^{1/2} \quad (3)$$

where t_c is the arrival time of the direct S_0 packet and t_d is the predicted end time of the first S_0 packet or the arrival of the first reflected S_0 packet if it precedes the predicted end time of the first S_0 packet. The window time values t_a , t_b , t_c , and t_d are computed from analytical functions which depend on both distance and frequency as explained in Section 3.3. The responses A_{p-c} and S_{p-c} can either be evaluated at a particular frequency or averaged over their respective frequency ranges for which these functions are defined.

In order to remove the effects of sensor degradation due to fatigue and static load, the percentage of signal degradation of the control PZT pairs are subtracted from

Table 1: Loading schedule, crack length, and percentage signal lost

Peak. Load (kN) - Strain ($\mu\epsilon$)	Crack Length (mm)	Load Cycles	Cum. Load Cycles	Eq. (1) Signal Loss (%)	Pair 1-4 Avg. % Change	Pair 1-4B Avg. % Change
57.8 - 3,335	1.67	6,000	6,000	-	26.7	39.7
57.8 - 3,335	5.21	8,000	14,000	12.1	10.5	13.2
48.9 - 2,822	13.96	4,000	18,000	1.8	-2.0	5.8
40.0 - 2,309	18.34	3,000	21,000	0.8	2.8	1.9
33.3 - 1,924	27.85	11,000	32,000	1.7	0.5	0.3
28.9 - 1,668	35.90	4,000	36,000	0.4	2.1	-2.4

the test PZT pair signals but only for identical load cases and/or increments of fatigue cycles. For example, the percentage change of the response S_{p-c}^* of PZT pair 1-5 corrected by reference PZT pair 1-4 between two cyclic load cases is computed from

$$S_{1-5}^* = \frac{\bar{S}_{1-5} - S_{1-5}}{\bar{S}_{1-5}} - \frac{\bar{S}_{1-4} - S_{1-4}}{\bar{S}_{1-4}} \quad (4)$$

where \bar{S}_{p-c} is the integrated response computed previous to S_{p-c} . For example, \bar{S}_{p-c} would be computed from the responses collected at 14,000 load cycles and S_{p-c} would be computed from the responses collected at 18,000 load cycles.

4 Results

4.1 Baseline Results

Before propagating fatigue cracks, responses are collected to form a healthy baseline for all four static loads: 0.45, 17.8, 26.7, and 35.6 kN. Figure 9 compares the peak amplitudes of signals collected from the healthy or undamaged structure to demonstrate the dependence of signal amplitude on applied static strain. This decrease in amplitude is due to the fact that PZTs are strain devices and the amplitude of the Lamb waves generated and received by PZTs is dependent on the strain they are currently experiencing. Responses between all PZT pairs are collected under all four static load conditions at every test increment listed in Table 1. Comparisons between data sets are only made under the same static load case and at each cyclic load increment. All cyclic loads applied have a fixed minimum to maximum ratio or load ratio R of 0.1.

The loads applied to initiate and propagate a crack in this experiment may not necessarily be representative of the actual loading an aircraft bulkhead would typically experience in flight or on the ground. The loads were selected to grow a crack in a timely manner. However, because high strain fields exist around crack tips and the PZTs are expected to be in close proximity to the cracks in geometrically constrained applications, the strains applied to the PZTs may not be too far from what could occur. In the end, this experiment does provide a valuable examination of the performance of a PZT-based SHM system in a high-strain and high-cycle fatigue environment, especially after severe PZT signal degradation.

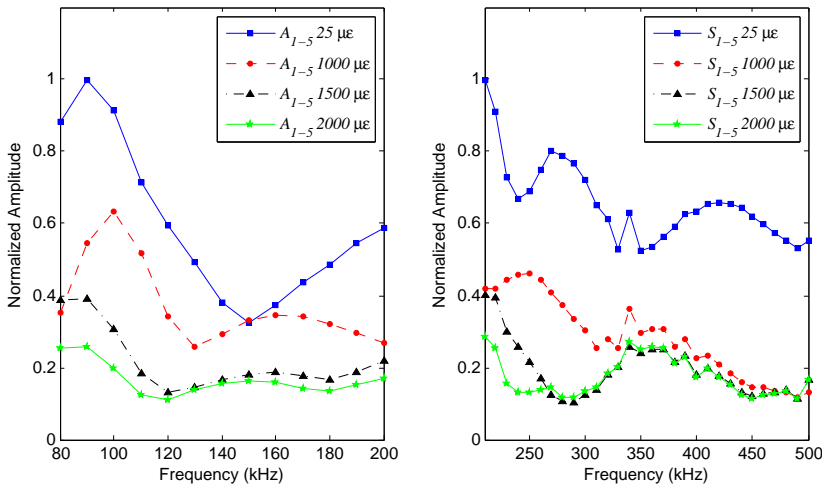


Figure 9: Comparison of normalized signal amplitude for initial static load - PZT pair 1-5

Although a crack was not visible after 6,000 load cycles in inspections using the 10X telescopic lens, the amplitude of the responses of the PZT pairs decreased considerably, confirming transducer and/or bond degradation due to high cyclic strain levels. Figures 10 and 11 show PZT pair 1-5 signals before and after the initial 6,000 load cycles. All of the PZTs experienced a peak strain of $3,335 \mu\epsilon$ which is close to the host structure's listed yield strain of $3,500 \mu\epsilon$ and far exceeds the PZT manufacturer's recommended maximum strain level of $1,100 \mu\epsilon$. Exposing the PZTs to strain levels that exceed the PZT manufacturer's static limit typically results in a variety of sensor and/or bond damage including cracking, disbond, and fracture [Blackshire, Martin, and Na (2007)] which permanently change the sensor's ability to generate and sense Lamb waves.

The average measured initial signal degradation between 80 and 500 kHz was

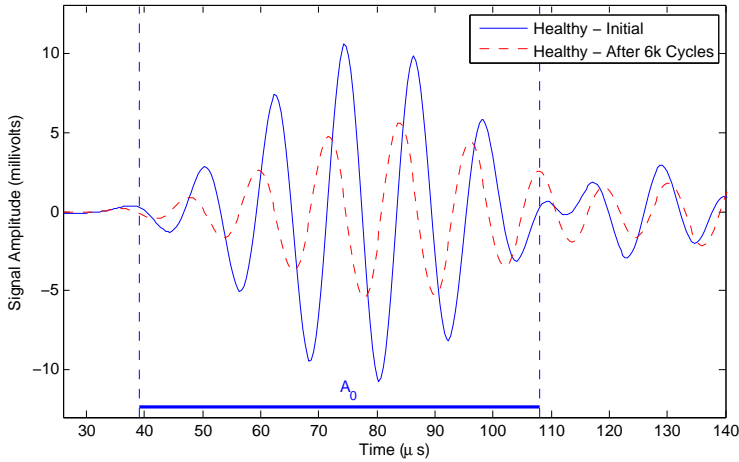


Figure 10: Comparison of 80 kHz signal measured for PZT pair 1-5 before and after initial 6k cycles

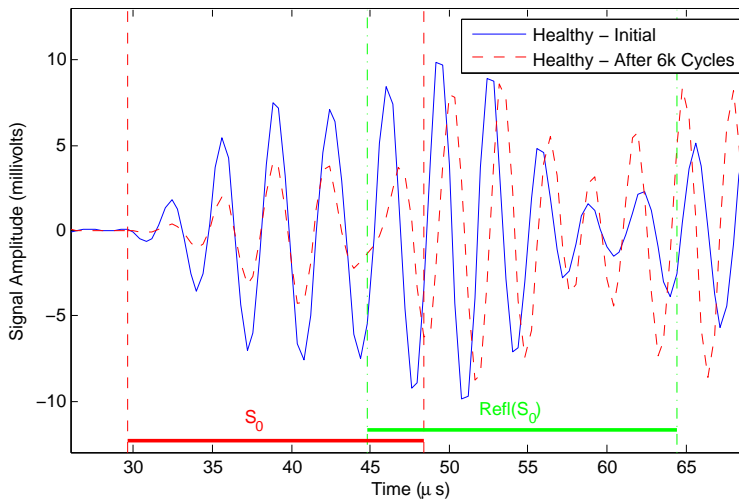


Figure 11: Comparison of 300 kHz signal for PZT pair 1-5 before and after initial 6k cycles

26.7% and 39.6% for PZT pairs 1-4 and 1-4B, respectively. These signal degradation values compare reasonably well with Kusaka and Qing’s [Kusaka and Qing (2003)] measured 20-30% degradation in signal amplitude after a single loading to 3,000 $\mu\epsilon$. Kuhn’s power model (column 5 of Table 1) also compares well with the

average measured changes in signal strength (columns 6 and 7 of Table 1) after the first 6,000 cycles in the frequency range 210 to 500 kHz. One benefit to Kuhn's power model is that it takes into account both the number of cycles and fatigue strain level, but it has a limited range of applicability. Even though Kusaka and Qing's measured results or Kuhn's power model could be applied to correct for the static and cyclic load effects seen in the majority of the responses collected in this research, a more direct approach of comparing relative changes in reference PZT pairs is applied. Direct subtraction of percentage changes in the reference PZT pair (1-4, 1-4B, 3-6, and 3-6B) responses are made from this point forward as opposed to using other researcher's measured results or equations. Because there exists a high level of variability in the amount of signal degradation due to transducer and/or bond damage, these more direct measurements appear to provide a more accurate measure of the signal changes due to high-cycle fatigue and applied static load. This approach of comparing relative signal changes is discussed further and demonstrated next.

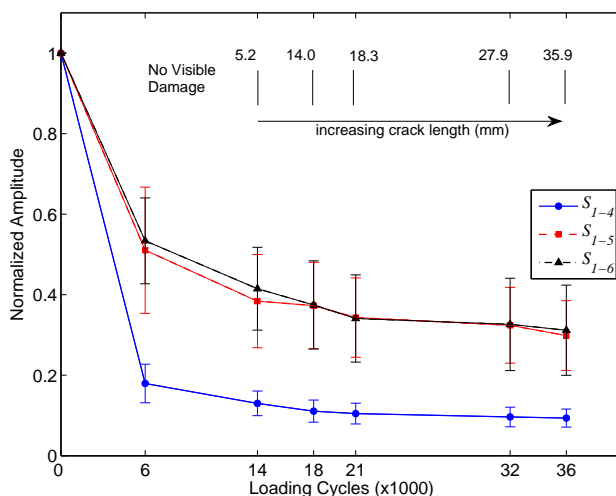


Figure 12: PZT pair responses averaged over 210 to 500 kHz under a 0.45 kN static load

4.2 Results with correction for load and high-cycle fatigue

Since a PZT-based pitch-catch approach is used to detect damage, test PZT pairs are selected based on the likelihood that the direct wave propagation path between two PZTs will intersect the crack and for minimal interference from reflected S_0 packets. For example, the paths between PZT pairs 2-5 and 2-5B include the rivet

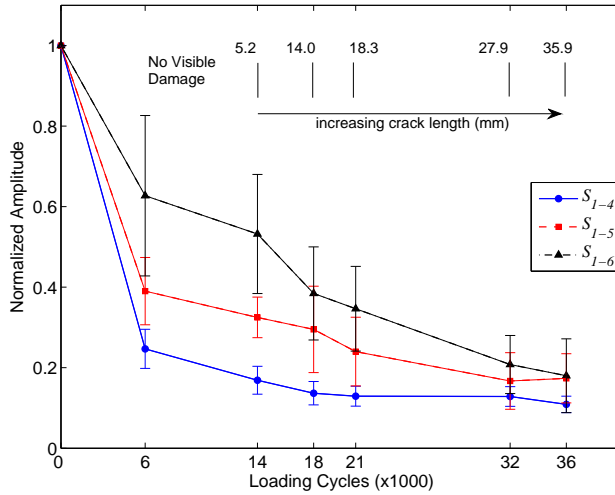


Figure 13: PZT pair responses averaged over 210 to 500 kHz under a 17.8 kN static load

hole and crack, once it is present. Conversely, the paths between PZT pairs 1-4, 1-4B, 3-6, and 3-6B are the farthest from the rivet hole and are not completely interrupted by the crack, and are therefore used as a control or reference to correct for the effects of fatigue and static loads.

Figures 12 and 13 show the PZT pair responses S_{p-c} as defined by Eq. (3) averaged over 210 to 500 kHz for different load cases. The figures include error bars (one standard deviation) to show the variability of the measured data. The y-axes do not have units because the data is normalized, and the x-axes have units of cycles which range from 0 to 36,000. Near the top of each figure, labeled vertical lines indicate the crack length and when data was collected. After 14,000 load cycles, the crack is present, and the peak cyclic load was reduced to control the rate of crack growth, as indicated in Table 1.

Figures 12 and 13 show that after 6,000 load cycles the averaged S_{1-4} responses degrade between 70 and 80%. The S_{1-5} and S_{1-6} responses also degraded between 30 and 60%. The responses collected from other PZT pairs after 6,000 load cycles typically showed similar levels of signal degradation; however, no correlation between the PZT pairs selected (test or reference) and magnitude of degradation was found. Signal degradation of this magnitude is attributed to both large strain levels and cyclic loading. If signal degradation of this magnitude is seen in a fielded SHM system, visual inspections of the “hot spot” would likely be conducted, and in this case, no fatigue cracks would be found. Eq. (4) is used to compute the response

degradation of PZT pairs 1-5 and 1-6 relative to reference PZT pair 1-4. The negative percentages, as seen in Figs. 14 and 15, indicate that the reference responses degraded more than the test responses.

After another 8,000 load cycles, the crack is visible, and Figs. 12 and 13 show that the averaged S_{1-5} and S_{1-6} responses degrade more when compared to the reference S_{1-4} responses. Higher relative percentages of signal degradation in the test PZT pairs is generally found in most data sets. When relative comparisons using Eq. (4) of the test PZT responses are made with respect to reference PZT responses, a positive trend in the percentage of signal degradation can be seen after 14,000 load cycles in Figs. 14 and 15. This positive trend indicates that the test PZT responses degraded more between load cycles than the reference PZT responses which could be attributed to the presence of the crack.

By comparing relative signal degradation S_{1-6}^* of PZT pair 1-6 in Figs. 14 and 15, a general trend of larger levels of relative signal degradation can be seen when data is collected with the test article under a larger static load. Even though static loads degrade PZT signal amplitude, as discussed earlier, there exists a general trend of larger reductions in signal strength as the crack propagates which may indicate that cracks may be easier to detect when the crack is open.

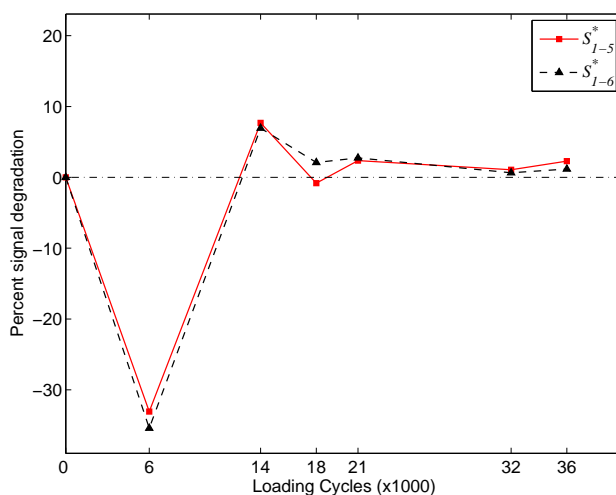


Figure 14: Signal degradation percentage S_{p-c}^* of PZT pairs 1-5 and 1-6 relative to reference PZT pair 1-4 under 0.45 kN static load

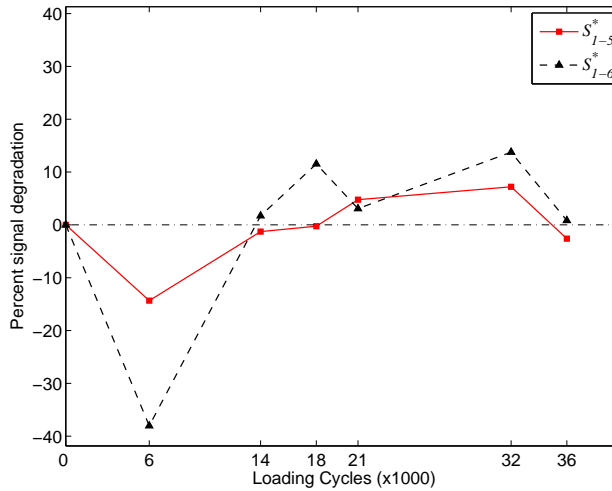


Figure 15: Signal degradation percentage S_{p-c}^* of PZT pairs 1-5 and 1-6 relative to reference PZT pair 1-4 under 17.8 kN static load

5 Conclusions

This paper presents results from an experiment designed to evaluate a damage detection approach for through-thickness fatigue cracks emanating from a rivet hole in an aircraft bulkhead. Fatigue cracks were propagated on both sides of a simulated rivet hole in a test plate after successive axial (tension-tension) loading cycles. PZTs are used in a “pitch-catch” approach to detect indications of damage using Lamb waves.

Detecting damage in a geometrically constrained environment is challenging because reflected waves can easily lead to false negative indications of damage. Therefore, a temporal windowing approach is applied to remove unwanted reflected signals. Because the PZTs are exposed to a high-cycle fatigue environment where the applied cyclic strains are above the manufacturer’s PZT static design limit, the PZT pair signal amplitude degrades significantly due to PZT damage and disbonding. In order to remove the effects of PZT damage due to high-cycle fatigue and static load, the relative changes in a reference signal are removed from the test signal to detect damage. The data shows that signals in the test PZTs typically degrade more than reference PZTs when the crack is present and obstructing the direct path. The data also shows a trend of slightly larger levels of signal degradation in the test PZT pairs when data is collected with the test article under larger static loads which would agree with the statement that cracks are easier to detect when the crack is

open. This may indicate that an SHM system using PZTs would be more useful while the aircraft is experiencing various loads in flight or on the ground.

Acknowledgement: The authors would like to acknowledge Mr. Mark Derriso (AFRL), Dr. Martin DeSimio (UDRI), Mr. Todd Bussey (AFRL), and Dr. Steven Olson (UDRI) for their suggestions, encouragement, and expert help throughout this experiment. We would also like to thank Mr. David Currie from Warner Robins AFB for his support in acquiring test articles. Finally, we would like to thank Mr. Jay Anderson (AFIT) for assistance in test setup.

References

Adams, D. (2007): *Health monitoring of structural materials and components*. John Wiley and Sons Ltd.

Blackshire, J.; Martin, S.; Na, J. (2007): The influence of bond material type and quality on damage detection for surface-bonded piezoelectric sensors. In *Proceedings of the 6th International Workshop on Structural Health Monitoring, Vol 1*. Stanford University, CA.

Kessler, S.; Amaratunga, K.; Wardle, B. (2005): An assessment of durability requirements for aircraft structural health monitoring sensors. In *Proceedings of the 5th International Workshop on Structural Health Monitoring*, Stanford, CA.

Kessler, S.; Shim, D. (2005): Validation of a Lamb wave-based structural health monitoring system for aircraft applications. In *Proceedings of the SPIE's 12th International Symposium on Smart Structures and Materials*, San Diego, CA.

Kuhn, J. (2009): *Changes in structural health monitoring system capability due to aircraft environmental factors*. PhD thesis, Air Force Institute of Technology, 2009.

Kusaka, T.; Qing, P. (2003): Characterization of loading effects on the performance of SMART layer embedded or surface-mounted on structures. In *Proceedings of the 4th International Workshop on Structural Health Monitoring, Stanford, CA*, pp. 1539–1546.

Lu, Y.; Ye, L.; Su, Z.; Yang, C. (2008): Quantitative assessment of through-thickness crack size based on Lamb wave scattering in aluminum plates. *NDTE International*, vol. 41, pp. 59–68.

Malkin, M.; Leonard, M.; Derriso, M.; Haugse, E. (2007): Hot spot monitoring: development of a framework for SHM design. In *Proceedings of the 6th International Workshop on Structural Health Monitoring*, pp. 786–792. Stanford University, CA.

Olson, S.; DeSimio, M.; Derriso, M. (2006): Analytical modeling of Lamb waves for structural health monitoring. In *Proceedings of the Third European Workshop on Structural Health Monitoring*, Granada, Spain.

Swenson, E.; Crider, J. (2007): Damage detection using Lamb waves for structural health monitoring on an aircraft bulkhead. In *Proceedings of the 6th International Workshop on Structural Health Monitoring*. Stanford University, CA.

Underwood, R. (2008): Damage detection analysis using Lamb waves in restricted geometry for aerospace applications. Master's thesis, Air Force Institute of Technology, 2008.

Underwood, R.; Swenson, E.; Soni, S. (2008): Structural health monitoring of aerospace applications with restricted geometry. In *Proceedings of SPIE's 15th International Symposium on Smart Structures and Materials*. San Diego, CA.

